

# An Open-Source Tool for Mapping War Destruction at Scale in Ukraine using Sentinel-1 Time Series

Olivier Dietrich<sup>1\*</sup>, Torben Peters<sup>1</sup>, Vivien Sainte Fare Garnot<sup>4</sup>, Valerie Sticher<sup>2</sup>, Thao Ton-That Whelan<sup>3</sup>, Konrad Schindler<sup>1</sup>, Jan Dirk Wegner<sup>4</sup>

<sup>1</sup>Photogrammetry and Remote Sensing, ETH Zurich.

<sup>2</sup>Department of Political Science, University of Zurich.

<sup>3</sup>International Committee of the Red Cross.

<sup>4</sup>EcoVision Lab, Department of Mathematical Modeling and Machine Learning, University of Zurich.

\*Corresponding author(s). E-mail(s): [odietrich@ethz.ch](mailto:odietrich@ethz.ch);

## Abstract

Access to detailed war impact assessments is crucial for humanitarian organizations to effectively assist populations most affected by armed conflicts. However, maintaining a comprehensive understanding of the situation on the ground is challenging, especially in conflicts that cover vast territories and extend over long periods. This study presents a scalable and transferable method for estimating war-induced damage to buildings. We first train a machine learning model to output pixel-wise probability of destruction from Synthetic Aperture Radar (SAR) satellite image time series, leveraging existing, manual damage assessments as ground truth and cloud-based geospatial analysis tools for large-scale inference. We further post-process these assessments using open building footprints to obtain a final damage estimate per building. We introduce an accessible, open-source tool that allows users to adjust the confidence interval based on their specific requirements and use cases. Our approach enables humanitarian organizations and other actors to rapidly screen large geographic regions for war impacts. We provide two publicly accessible dashboards: a [Ukraine Damage Explorer](#) to dynamically view our pre-computed estimates, and a [Rapid Damage Mapping Tool](#) to easily run our method and produce custom maps.

The Russian invasion of Ukraine in February 2022 escalated a simmering conflict, which had previously seen unofficial Russian involvement limited to the country’s eastern regions, into a full-scale war between the two countries. Russian troops crossed into Ukraine from multiple fronts and advanced through the country, reorienting their geographical focus as Ukrainian forces mounted an unexpectedly fierce resistance. As the Russian troops advanced, they subjected numerous cities

to heavy shelling and destroyed critical infrastructure. Millions of Ukrainians fled their homes as damage and destruction spread throughout the country. Two years into the conflict, the war has caused hundreds of thousands of casualties and inflicted billions of dollars in damages to Ukraine’s infrastructure [1, 2].

The fast-paced early stages of the Russia-Ukraine war serve as a stark reminder of the challenges humanitarian organizations encounter

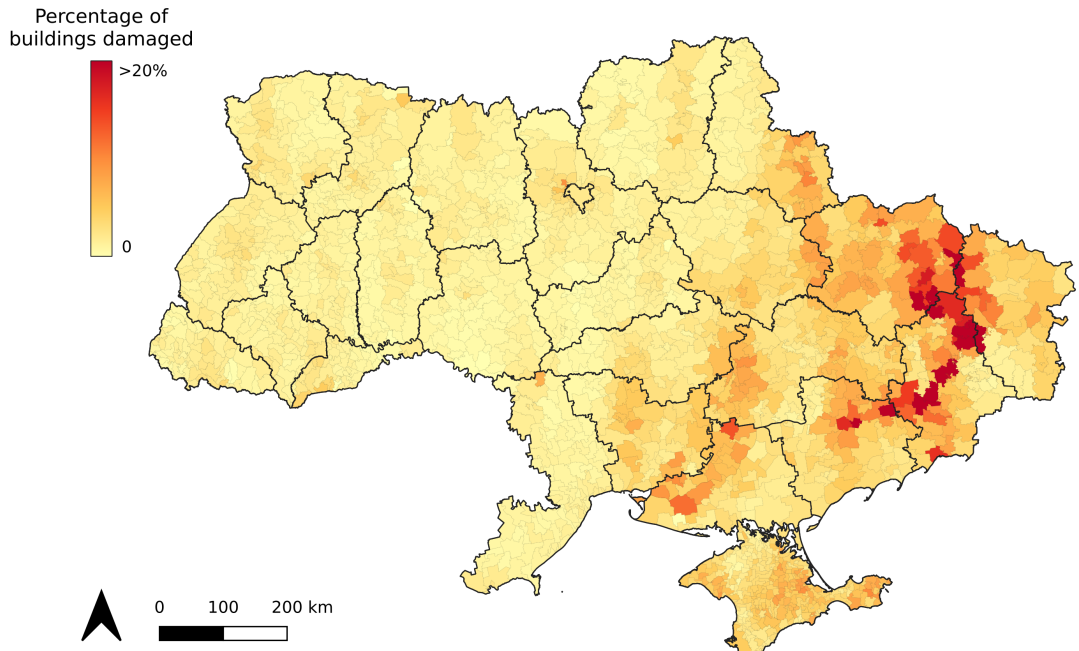


**Fig. 1** Percentage of buildings likely damaged within the first two years of the war, aggregated by *hromadas*. The predictions were thresholded at 0.64, and only buildings larger than  $50\text{ m}^2$  were considered.

when monitoring ongoing armed conflicts in real-time. Even in less intense conflicts, like the war in Eastern Ukraine before the full-scale Russian invasion, violence can flare up unexpectedly, and minor incidents may trigger escalatory dynamics. Thus, regardless of a conflict's intensity, it is essential for humanitarian organizations to have a complete and up-to-date understanding of the situation on the ground to effectively support those most affected by the conflict. However, the task of maintaining such an overview is challenging, especially with limited resources. The difficulty is compounded when conflicts affect large geographic areas, persist over long periods of time, or occur in regions that are inaccessible due to security concerns.

## Satellite-Based War Damage Assessments

To overcome these challenges, organizations have increasingly relied on satellite imagery to supplement on-the-ground monitoring. Although satellite images lack contextual details and a narrative dimension, they provide snapshots of the conditions on the ground, making it possible to observe

how the situation evolves and how destruction spreads. Furthermore, satellites offer global coverage and automatic data acquisition, which is essential for monitoring large, remote, or inaccessible areas. The primary technique to perform damage assessments from satellite imagery is manual analysis of very high-resolution (VHR) optical images. As it involves the visual comparison of expensive commercial imagery, that method is labor-intensive and costly. Despite its accuracy and reliability, it depends on the availability of VHR data and does not scale to conflict zones that are large and that require long-term monitoring.

Nowadays, the analysis of satellite imagery with machine learning offers opportunities to automate parts of the labor-intensive remote monitoring process. Multiple studies have demonstrated the efficiency and effectiveness of this approach for assessing building damage. The most accurate methods currently involve applying deep neural networks to VHR optical data [3–6], often leveraging large dedicated datasets [7]. These approaches primarily focus on natural disasters, which typically require a one-time analysis of relatively localized, clustered damages. In contrast, armed conflicts can last for months, years, or even

decades, resulting in spatially dispersed and gradually increasing destruction. Consequently, they require continuous monitoring over extended periods, so that automated change detection can on the one hand bring larger benefits, but on the other hand is more challenging [8].

Recent work has begun to apply research specifically to the task of assessing building destruction induced by armed conflicts. In a seminal study, Mueller et al. [9] trained a CNN with VHR optical imagery and labels from UNOSAT [10] to assess war-induced building destruction in Syria, leveraging the persistent nature of war damage over time due to the absence of reconstruction efforts amidst ongoing fighting. However, accessing VHR optical imagery for conflict zones is costly, as commercial sources typically do not provide free access to their database in these situations [11], unlike after natural disasters [12, 13]. As such, relying on repeated, large-area coverage with VHR images to monitor armed conflicts at scale is unrealistic for most actors, which recently has prompted studies based on moderate-resolution imagery [14].

Beyond optical images, Synthetic Aperture Radar (SAR) imagery offers a promising alternative. SAR is an active sensor system that illuminates the Earth's surface with microwave pulses and captures the backscattered signals. It is sensitive to geometrical changes on the ground, such as destroyed buildings. Unlike its optical counterpart, SAR can operate at any time of day (respectively, night) and is largely unaffected by clouds. SAR-based change detection can be divided into amplitude-based methods such as the recent PWTT [15], and phase-based methods such as the popular coherence change detection (CDD) [16, 17]. Due to the sub-meter wavelength of SAR, phase-based methods can detect changes much smaller than the pixel resolution [18]. On the downside, these techniques rely heavily on stable pre-event coherence, which can be problematic with practical, operational satellite SAR systems. Furthermore, creating reliable coherence maps is a complex process that involves a loss of resolution.

## Open-Source Tool for Mapping War Impact

In this work, we introduce an easy-to-use, open-source war impact mapping tool based on SAR

amplitude data and demonstrate its effectiveness through a comprehensive building damage assessment across Ukraine. Our solution leverages existing, point-wise damage maps from UNOSAT [10] and public, open SAR imagery from the Sentinel-1 mission [19]. Harnessing the parallel computing capabilities of Google Earth Engine (GEE) [20], we train a model to estimate the likelihood of war-related changes from paired time series of Sentinel-1 backscatter. We choose a fixed one-year interval in 2020 as our reference period and iteratively generate damage likelihood maps for 3-month periods ranging from February 2021 up to February 2024. Our model, based on the Random Forest algorithm, allows for straightforward deployment on GEE. In a second processing step, we intersect the per-pixel maps with publicly available building footprints from Overture Maps [21] to generate a damage estimate per building. Our tool produces maps of war damage at very low cost and enables continuous country-scale monitoring. These maps can serve both as a basis for large-scale, aggregated assessments and as guidance to focus manual verification efforts for individual settlements or buildings. We offer two public online dashboards: In the [first one](#), users can dynamically view and explore the pre-computed damage maps described in the following. The [second one](#) allows users to run our method themselves for their desired locations and time periods and create custom maps.

The key advantages of our approach are its scalability and ability to transfer to different geographic contexts. Using commercial VHR imagery for regular screening across entire conflict zones is not viable for humanitarian organizations [22], because it would be too resource-intensive, in terms of both direct data cost as well as infrastructure for data download, storage, and compute. By utilizing moderate-resolution satellite images that are free of charge and acquired with short, regular revisits, we enable a more sustainable monitoring approach. The use of SAR imagery has the additional advantage that it can be expected to be transferable to other conflict contexts, including those with different architectural patterns and/or with even more frequent cloud cover. The proposed method is also fast, reproducible, and easy to adapt, even for users who are not experts in remote sensing or image analysis. We believe that our work could be a valuable and accessible

resource and could be used to screen large conflict areas beyond our specific application case.

## Results

### Evaluation

We first evaluate our model’s predictions against additional damage assessments excluded from the training set (see Fig. 4 for the geographic distribution of our test set). The UNOSAT-labeled locations are compared to the corresponding raw pixel predictions of the model. True positive and false negative rates are counted in the 3-month periods from 2022 (after the invasion), and true negative and false positive rates are counted in the periods from 2021 (before the invasion). To guard against potential shifts between the point labels and the satellite tiles, *e.g.* due to high incidence angles or inaccurate annotation, we compare to the maximum predicted damage probability in a  $3 \times 3$  pixel window centered at the reference label. We obtain an F1-score of 73.9% for the damaged class and an AUC of 80.3%. As a baseline we also show results for the pixel-wise T-test (PWTT) method [15], using the same evaluation protocol. Our method consistently outperforms that baseline, see Table 2. For details about the comparison see Appendix B.

The evaluation of held-out validation data also helps establish an appropriate threshold for distinguishing between damaged and undamaged pixels. Indeed, while the model has been trained on a balanced dataset, the actual distribution of damaged versus undamaged pixels is highly skewed, and the prevalence of undamaged pixels in the test set means that thresholding at damage probability 0.5 will cause a significant number of false alarms. We employ the  $F_\beta$  score, a weighted harmonic mean of precision and recall, where recall has  $\beta$  times the weight of precision, to fine-tune this threshold.

$$F_\beta = \frac{(1 + \beta^2) \cdot \text{precision} \cdot \text{recall}}{\beta^2 \cdot \text{precision} + \text{recall}} \quad (1)$$

In the real-world setting, most pixels are undamaged even in heavily affected locations, we optimize the  $F_{0.2}$ -score. With this choice, we find an optimal confidence threshold of 0.64. For details about the threshold optimization see Appendix C. With that value more false positives

are suppressed and precision for the damaged class reaches 0.889, at the cost of a lower recall of 0.409. We point out that there is an inherent trade-off between missed detections and false alarms, and the right threshold depends on the application task. Our dashboard allows the user to adjust it with a slider and explore how different thresholds affect the estimates. Table 1 reports results for the settings described above, with a confidence threshold of 0.5 and 0.64.

### Close-Ups

We use Chernihiv, one of the cities in our test set, to qualitatively illustrate the performance and limitations of our approach. Fig. 2 shows both heatmaps of damage probability and per-building maps after post-processing with building footprints. Inset A highlights one limitation of using building footprints, as the leftmost damage label has been correctly predicted in the heatmap but does not have a corresponding footprint. Inset B illustrates how the model can detect correct patterns of destruction, even for small structures. However, some labels (*e.g.*, center-top) are completely missed, likely because the affected building volume was too small to be visible at Sentinel-1 resolution. Inset C shows both how multiple UNOSAT labels can fall within a single footprint, and how taking the mean prediction over a partially affected building footprint can discard some correct predictions (third point from the bottom). In the main figure, outside the boundaries of UNOSAT analysis, we observe agricultural fields wrongly identified as damaged in the heatmap. This is expected, since our model has not been trained for patterns that occur outside of settlement areas, and illustrates the need to post-process the raw heatmaps with settlement masks or building footprints.

### Web-based Tool

We have developed a web application based on Google Earth Engine (GEE) to facilitate rapid reproduction of our results and enable the generation of new maps without any local software installation. The application features a user-friendly dashboard (Fig. 3) that provides the functionality to perform damage assessment for a user-specified region of interest and using user-defined pre- and post-event observation periods. The predicted

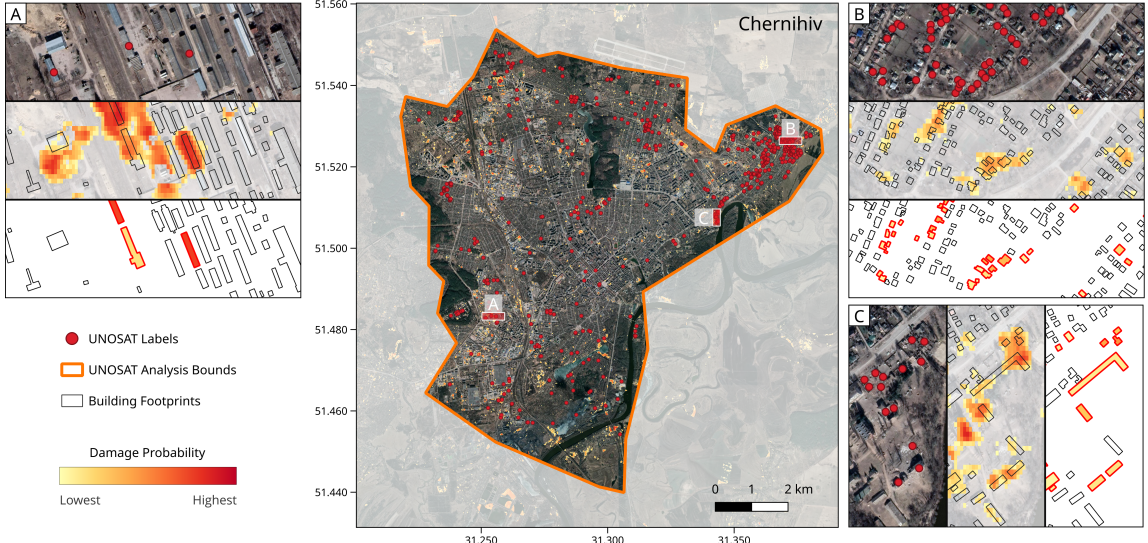


**Fig. 2** Building damage estimate for Chernihiv (standard confidence threshold 0.64), aggregated over the first two years of conflict. For clarity, we only present the damage heatmap in the main figure, while three zoomed insets show building-level predictions. Red dots represent UNOSAT annotations indicating buildings marked as either *destroyed* or *severely damaged*. The VHR satellite layer is displayed solely for visualization, all results are derived from 10m-resolution Sentinel-1 images. Readers are encouraged to explore the maps on the interactive [dashboard](#). Sources: Google Earth/Maxar satellite imagery, Overture Maps building footprints, UNITAR/UNOSAT damage annotations.

Label	Precision	Recall	$F_1$	$F_{0.2}$	Accuracy	AUC
Damaged	69.7 (88.9)	78.7 (40.9)	73.9 (56.0)	70.0 (85.1)	80.7 (77.7)	80.3 (69.1)
Undamaged	87.8 (75.6)	81.8 (97.3)	84.7 (85.1)	87.6 (76.3)		

**Table 1** Quantitative performance with respect to UNOSAT labels (at previously unseen locations), using a confidence threshold of 0.5. Values in parentheses indicate performance at the optimal threshold of 0.64, maximizing the  $F_{0.2}$  score for the *damaged* class. The *undamaged* class is evaluated using the same locations, but acquisition windows before the full-scale invasion. All metrics are given as percentages.

Method	Recall	$F_1$	AUC
PWTT[15]	76.3	68.4	75.7
Ours	78.7	73.9	80.3

**Table 2** Comparison of our method with the PWTT [15], with the latter calibrated for Ukraine. Metrics were computed on our test set, using the same settings for both approaches. All metrics are given in percentages.

maps can also be exported as raster files directly from the interface (subject to GEE restrictions on download size). Furthermore, the dashboard

includes a visualization tool that enables pixel-by-pixel examination of Sentinel-1 time series data at any desired location.

## Country-wide Analysis

To illustrate the scalability of our approach, we have run damage assessments over the entire country. Our analysis indicates that over 500,000 buildings in Ukraine, or approximately 3.5% of all buildings, have likely sustained damage during the first two years of conflict. This estimate only accounts for buildings larger than  $50\text{ m}^2$ . Fig. 1 shows the percentage of buildings likely damaged within the first two years of the war, aggregated by *hromadas*, which is the finest administrative



**Fig. 3** Screenshot from the [dashboard interface](#), displaying damage estimates for a region in Mariupol, alongside the Sentinel-1 time series visualizer.

division in Ukraine that covers the entire territory. For the most impacted *hromadas* with over 10,000 buildings—Bakhmutyska, Marinska, and Popasniyska—damage rates reach 47.1%, 32.1%, and 29.0%, respectively. We observe that this pattern of destruction correlates with the course of the war, the eastern side of the country having been a battlefield for months, while the western part has been relatively spared. For a subset of  $\approx 1.8M$  buildings in our dataset, we were able to retrieve meta-data about the building function (such as "residential" or "medical") from the OpenStreetMap catalog. Table 3 summarizes the damaged fractions for different building functions. In this preliminary analysis, we did not find any country-wide patterns that would suggest that certain building types are more prone to war damage than others. Note a more detailed study is needed to confirm or reverse this finding, as biases in the definition and distribution of the available OpenStreetMap building function labels could influence the result.

## Discussion

Knowing where and when war-related building damage has occurred is essential for humanitarian organizations to assist populations affected by armed conflicts. The open-access remote monitoring tool that we introduce in this article allows

OSM Class	# Damaged	% Total
Residential	70,925	4.5
Industrial	4,207	6.6
Outbuilding	851	2.3
Commercial	1,576	4.7
Education	765	4.0
Agricultural	1,127	6.0
Service	368	4.3
Religious	186	2.3
Medical	152	4.3
Civic	145	5.7
Transportation	133	6.2
Entertainment	11	3.5
Military	7	4.8

**Table 3** Number of buildings damaged per OSM class across Ukraine. The footprints with OSM class information represent a subset of 11.9% of all building footprints analyzed.

users to rapidly gain an overview of war-related impact. It can also supplement interactive damage mapping and serve as a pre-filtering step to guide reliable, but resource-intensive photo-interpretation by human operators. We have demonstrated the effectiveness of our tool by conducting a comprehensive building damage assessment across Ukraine, showing how war-related destruction has spread throughout the country. The retrieved distribution of damaged buildings broadly reflects the frontlines of the conflict, with the most severe destruction concentrated in areas that experienced prolonged and intense fighting.

While so far only tested in Ukraine, we expect our method to transfer well to other geographical contexts, due to the properties of both the underlying Sentinel-1 SAR data and the Random Forest classifier used to analyze it.

## Limitations

While our tool for screening conflict-related building damage proved effective, it is important to acknowledge its limitations and interpret its outputs accordingly. In this context, we again highlight that the purpose of our method is to complement existing damage mapping solutions with a scalable screening component, not to replace human photo-interpretation or ground-based damage reports.

**Classification Threshold:** One key limitation is the sensitivity of the quantitative estimates to the selected confidence threshold. As a pragmatic solution, our tool provides a slider that lets the user adjust the threshold according to the precision/recall trade-off needed for a specific use case. For example, a higher threshold may be appropriate to gather spatially coarse aggregate statistics about destruction patterns as in 1, whereas a lower threshold might better support the search for individual, hitherto overlooked damages.

**Dependence on External Data:** Our model has specifically been trained on building data and therefore presupposes that settlement or building boundaries are available to mask out areas without human settlements (e.g., agriculture, forest, etc.), which would otherwise cause many false positives. We found that it is sufficient to utilize standard, global land cover maps[23], settlement layers[24], or building footprints. Still, the reliance on such external sources is a potential source of error (see Appendix E for possible issues specific to building footprints).

**Choice of Reference Period:** To have a common pre-event reference for both negative and positive samples, we used the year 2020 as a fixed reference period throughout this work. This means, however, that the temporal gap between the pre-event and post-event periods can be rather large; giving rise to mis-classifications due to surface changes other than war damage, e.g., construction. Ideally, a future version of the tool

would integrate context knowledge about the conflict to minimize the temporal gap between the pre- and post-event observation periods.

**Reference Data:** Finally, our supervised learning approach necessitates a sufficient volume of reference data. Despite existing calls for large-scale datasets and open data programs dedicated to armed conflicts [11], such resources remain limited. Data availability varies significantly between different contexts: for some conflicts, e.g. the wars in Ukraine and Gaza, quite a lot of damage data is available; whereas there may be very little information about building damages in conflicts that receive less public attention. It is precisely in these under-reported conflicts that automated analysis could have the biggest impact. By offering an accessible open-access tool based on public satellite data, we hope to take one step toward a global monitoring solution. But to get there it will likely be necessary to collect at least some training data that represent the building patterns and imaging conditions of regions with under-reported conflicts.

**Processing time and user experience:** In principle, the proposed method is fast. Still, when running the web tool it may take several minutes to display the result, due to the technical overheads of GEE. As an alternative, one may download the corresponding image tiles and process them locally with the provided code. In the future, we hope to further accelerate the online tool.

## Policy Implications

The combination of free Earth observation data and machine learning offers a promising route toward automated war damage monitoring, complementing interactive mapping and on-the-ground surveys.

But there is inherent uncertainty in predicting damage probabilities from SAR image patterns at 10 m resolution, and users should understand this and align their expectations with what such methods can deliver. Our approach is perhaps best suited to obtain a high-level overview of how damage spreads across time and space. Beyond scientific goals like tracing the development of the conflict, this should often be enough to understand where populations are affected. At the same time,

our method cannot confirm damage to an individual building, meaning that it is not directly comparable to assessments based on VHR imagery, ground-based photography, witness reports, etc. Importantly, the automatic large-scale approach and reliable local evidence are complementary: satellite damage maps can identify regions that warrant the effort to gather detailed, reliable evidence.

Post-processing the model outputs with additional data sources, as demonstrated for Ukraine with building footprints, adds an important dimension of information. Future research could seek to assimilate further sources of information, for instance, news reports or social media. Despite the inherent biases of such sources [25], they contain a wealth of complementary information that could be harvested, adding contextual knowledge and narrative depth to maps derived purely from satellite images. For example, attacks on residential buildings carry different policy implications if these buildings are inhabited than if civilians have fled an area in anticipation of strikes. Of course, even when data sources are combined to enhance the information derived from satellite images, contextual knowledge offered by observers and humanitarian organizations remains crucial for decision-making.

Beyond immediate humanitarian action, our large-area war impact maps are potentially useful also to support other efforts to remedy the consequences of armed conflicts, such as planning, prioritization, and resource allocation during reconstruction efforts. In terms of scientific inquiry, wall-to-wall, spatially explicit data allows for fine-grained geospatial analysis of conflict dynamics, which at present relies almost entirely on events derived from news articles. Building damage information obtained through our approach can serve as an additional data source that is complementary to the more commonly used metric of battle-related fatalities.

## Methods

### Data

#### Reference Damage Assessments

To the best of our knowledge, the only public, georeferenced datasets that provide building-level

damage information for Ukraine are the UNOSAT maps [10]. They are based on commercial VHR imagery, where analysts manually compare pre- and post-event images using a standardized damage scale. To maximize the chances that these damages produce discernible changes in the SAR imagery, we only keep the two most severe damage levels, *i.e.* *destroyed* or *severely damaged*, and discard the others. We aggregate all available UNOSAT maps for Ukraine into a dataset consisting of 10,934 unique entries, distributed across 18 different areas of interest (AOIs) as depicted in Fig. 4. Importantly, these labels are attached to geo-coordinates, without any relation to concrete events. We, therefore, lack information on both the spatial extent and the precise date of the destruction, all that is known is that it happened between the pre- and post-event dates. For the present work, we further restrict this interval by assuming that no damage occurred before the onset of the invasion on February 24, 2022. We point out that this assumption may not strictly hold in the eastern regions, particularly Luhansk and Donetsk oblasts. A detailed summary of our dataset can be found in Appendix A.

### SAR Image Time Series

We use freely available SAR data from the Copernicus Sentinel-1 mission [19], consisting of two satellites equipped with C-band SAR instruments and moving in the same orbital plane, phased 180° apart. This setup originally allowed for global coverage with a revisit period below 6 days anywhere on Earth. Unfortunately this period has doubled to up to 12 days since the technical failure of Sentinel-1B in December 2021. For our study, we only use data from Sentinel-1A to maintain consistent temporal resolution. We utilize the Ground Range Detected (GRD) product available on GEE, consisting of log-amplitudes for the VV and VH polarizations, resampled at 10 m. Internally, GEE automatically preprocesses every tile with precise orbit correction, border and thermal noise removal, radiometric calibration, and terrain correction. We do not add any further preprocessing.

### Building Footprints

We leverage the building layer from the Overture Maps Foundation’s Open Map Data [21],

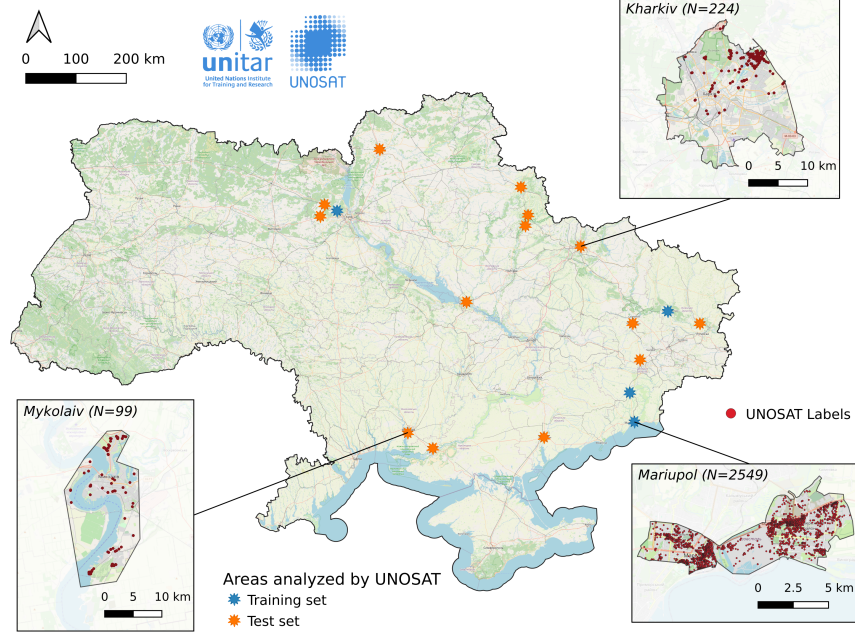


**Fig. 4** Overview of the 18 areas analyzed by UNOSAT in Ukraine.

which combines building footprints from diverse sources. In Ukraine, this equates to a total of 26.5M buildings, with 24.7% coming from Open-StreetMap’s crowd-sourced database [26] and the remaining 20M from Microsoft’s Global Building Footprints [27]. We note here that these building footprints have their own limitations. E.g., Open-StreetMap data may be outdated, and Microsoft footprints, retrieved from VHR optical imagery with a deep learning model, may suffer from missing buildings and geometric inaccuracies, particularly for small buildings. Considering the resolution of Sentinel-1 we only take into account the 15M buildings that exceed  $50 \text{ m}^2$  in surface area, *i.e.*, they are larger than half a pixel. Appendix E illustrates some of these limitations.

## Definition of Time Intervals

For clarity, we first define the temporal acquisition windows used in our study. Time interval  $T_0$  covers one year from Feb. 24, 2020 until Feb. 23, 2021. The subsequent intervals  $T_1$  to  $T_{12}$  represent consecutive 3-month time windows, with  $T_1$  ranging from Feb. 24, 2021 to May 23, 2021, and the last interval  $T_{12}$  spanning Nov. 24, 2023 to

Feb. 23, 2024. As such, intervals  $T_1$  to  $T_4$  represent the year preceding the invasion, while  $T_5$  to  $T_{12}$  represent the two years following it.

## Machine Learning Framework

### Time Series Extraction

For each location marked by UNOSAT, we stack the corresponding Sentinel-1 tiles and extract all backscatter values, for both the VV and VH polarizations. Limiting the training to the points annotated by UNOSAT corresponds to a fully supervised learning scheme where the target value is known for every training example. As the annotated points may be slightly offset due to large nadir angles or inaccurate annotations, we average the backscatter over a  $3 \times 3$  pixel window centered at the marked location. By relying only on this minimal neighborhood we disregard spatial context. We found that the time series signal carries most of the information relevant to our analysis, presumably because conflict-induced building damages are mostly small and localized. Per-pixel processing also scales particularly well on parallel processing architectures like the one underlying GEE.

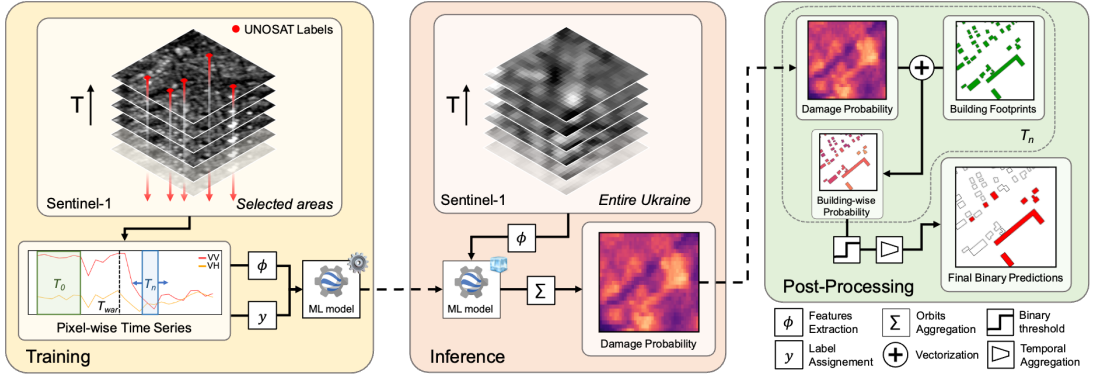


**Fig. 5** Overview of our machine learning framework. For training (left), we use per-pixel Sentinel-1 time series extracted at the location of UNOSAT point annotations. The model is fed with a pair of time series from the same location. The first one spans a fixed 12-month time interval  $T_0$  from 2020, and the second one spans one of the 3-month time intervals  $T_n$  between 2021 and 2023. Both time series are encoded with a custom features extractor, and damage labels are dynamically assigned according to  $T_n$ . At inference time (center), the model generates a damage probability heatmap valid at  $T_n$  and spanning the entire country, aggregating the predictions of different Sentinel-1 orbits. The raw damage probabilities are intersected with building footprints. For the final map the estimates for different time intervals  $T_n$  are thresholded and aggregated.

Importantly, Sentinel-1 has the typical side-looking viewing geometry of SAR sensors, where the same location may look very different depending on the incidence angle and orbit direction. We therefore extract the backscatter values independently for each orbit, resulting in 2 to 4 time series per UNOSAT reference point. Overall, we obtain 33,304 distinct time series, denoted as  $x_i^o$ , where  $i$  denotes the ID (respectively, location) and  $o$  is the orbit index.

## Classification

We formulate damage mapping as a supervised, binary classification. From each time series, we extract two segments: the fixed reference period  $x_{i,\text{ref}}^o$  and the assessment period  $x_{i,\text{new}}^o$ . The task of the classifier is to estimate the probability that a war-related change has occurred in the time window between the two segments. For each segment and each band, we extract a set of  $N$  statistical features and combine them into a final feature vector denoted as  $\phi(x_i) \in \mathbb{R}^{4N}$  that forms the input to the classifier. This strategy has several advantages. First, by fixing the reference period before the start of the war one can ensure that it represents the state without any war-induced damages. Second, extracting fixed-length segments makes the method independent of the overall conflict duration. Third, using multiple different assessment periods greatly increases the number of

training examples and also helps to make the model robust against seasonal variations.

As classification algorithm, we use a Random Forest as implemented in the SMILE library [28], since that algorithm is available off-the-shelf in GEE, facilitating large-scale deployment. For every input feature vector the model outputs a score  $\hat{y}_i^o \in [0, 1]$ , which can be interpreted as the likelihood that war-induced damage has happened between the associated reference and assessment periods. At inference time, we compute the overall damage probability map by averaging the estimates from different orbits,  $\hat{y}_i = \frac{1}{N_o} \sum \hat{y}_i^o$ .

## Training Details

We perform all computations directly in GEE. We train the model on the four AOIs with the highest numbers of reference labels, Mariupol, NW Kyiv, Rubizhne, and Volnovakha. Together they represent 75.0% of all UNOSAT annotations and 82.6% of all backscatter time series. The remaining fourteen AOIs are reserved for evaluation, ensuring geographic diversity (see Fig. 4). We choose  $T_0$  as a fixed reference period and randomly use periods from  $T_1$  to  $T_8$  (e.g. spanning one year before and after the beginning of the war) as assessment periods.

The label  $y_i$  is dynamically assigned to each  $x_i$  based on the end date  $t_{max}$  of the assessment

period:

$$y_i = \begin{cases} 0 & \text{if } t_{max} \leq t_{invasion}, \\ 1 & \text{if } t_{max} > t_{unosat}, \\ -1 & \text{otherwise} \end{cases} \quad (2)$$

where  $t_{invasion}$  is 2022-02-24, the day the invasion was launched; and  $t_{unosat}$  is the acquisition date of the post-event image used for annotation by UNOSAT. All time series with  $y_i = -1$  are discarded because we cannot determine whether they contain the damage event. We transform  $x_i$  into  $\phi(x_i)$  using the following seven summary statistics: minimum, maximum, mean, median, standard deviation, kurtosis, and skewness. Finally, we configure the Random Forest to use 100 decision trees, with *minLeafPopulation* set to 3 and *maxNodes* set to 10,000. These values ensure sufficient robustness while remaining within the computational budget permitted by GEE.

## Country-wide Inference

After model training, we leverage the parallel computing capabilities of GEE to generate damage probability maps for the entire country. We compute one map for each period seen during training, as well as four additional maps for  $T_9$  to  $T_{12}$ , the assessment periods between 2023 and February 2024. Each map, in EPSG:4326 projection and stored in UInt8 format, has an extent of 88,867×201,284 pixels and a file size of 17.88GB.

## Post-Processing

To quantify the impact of the war on the Ukrainian building stock, we cross-reference our maps with the building footprints sourced from Overture Maps [21]. For each building  $b_j$  and each period  $T_n$ , we assign a damage likelihood  $\hat{y}_{j,T_n}$  by averaging the likelihood values of all pixels that fully or partially overlap the footprint, weighted by the overlap fraction:

$$\hat{y}_{j,T_n} = \sum_i w_{ij} \hat{y}_{i,T_n} \quad (3)$$

Here  $\hat{y}_{i,T_n}$  represents the model output at pixel  $i$  for the period  $T_n$ , and  $w_{ij}$  is the proportion of that pixel that falls within  $b_j$ . By construction, this process also discards all damage estimates that fall

outside of buildings, e.g. in agricultural areas or forests.

To obtain a final estimate of the number of buildings impacted over the first two years of the war, we aggregate the maps for the relevant assessment periods with the following rule:

$$\hat{y}_j = \begin{cases} 1 & \text{if } \max(T_{[5,12]}) \geq t \text{ and } \max(T_{[1,4]}) < t \\ 0 & \text{otherwise} \end{cases} \quad (4)$$

## References

- [1] Kyiv School of Economics. Russia will pay project. URL <https://kse.ua/about-the-school/news/155-billion-the-total-amount-of-damages-caused-to-ukraine-s-infrastructure-due-to-the-war-as-of-january-2024/>. Accessed 2024-03-14.
- [2] World Bank. Ukraine - third rapid damage and needs assessment (RDNA3): February 2022 - december 2023. World Bank Group (2023). URL <http://documents.worldbank.org/curated/en/099021324115085807/P1801741bea12c012189ca16d95d8e2556a>.
- [3] Xu, J. Z., Lu, W., Li, Z., Khaitan, P. & Zaytseva, V. Building damage detection in satellite imagery using convolutional neural networks. *arXiv preprint arXiv:1910.06444* (2019). URL <https://arxiv.org/abs/1910.06444>.
- [4] Lee, J. *et al.* Assessing post-disaster damage from satellite imagery using semi-supervised learning techniques. *arXiv preprint arXiv:2011.14004* (2020). URL <https://arxiv.org/abs/2011.14004>.
- [5] Gholami, S. *et al.* On the deployment of post-disaster building damage assessment tools using satellite imagery: A deep learning approach 1029–1036 (2022).
- [6] Kaur, N., Lee, C.-C., Mostafavi, A. & Mahdavi-Amiri, A. Large-scale building damage assessment using a novel hierarchical transformer architecture on satellite images. *Computer-Aided Civil and Infrastructure Engineering* (2023).
- [7] Gupta, R. *et al.* xBD: A dataset for assessing building damage from satellite imagery. *arXiv preprint arXiv:1911.09296* (2019). URL <https://arxiv.org/abs/1911.09296>.
- [8] Sticher, V., Dietrich, O., Pfeifle, B. & Wegner, J. D. Watching armed conflicts from space. *CSS Analyses in Security Policy* (2024).
- [9] Mueller, H., Groeger, A., Hersh, J., Matranga, A. & Serrat, J. Monitoring war destruction from space using machine learning. *Proceedings of the National Academy of Sciences* **118** (2021). URL <https://doi.org/10.1073/pnas.2025400118>.
- [10] UNOSAT. United Nations Satellite Center. URL <https://unosat.org/about-us/>.
- [11] Bennett, M., Van Den Hoek, J., Zhao, B. & Prishchepov, A. Improving satellite monitoring of armed conflicts. *Earth's Future* **10**, e2022EF002904 (2022).
- [12] MAXAR. MAXAR open data program. URL <https://www.maxar.com/open-data>. Accessed: 2024-03-14.
- [13] Planet. Planet disaster data program. URL <https://www.planet.com/disasterdata/>. Accessed: 2024-03-14.
- [14] Hou, Z. *et al.* War city profiles drawn from satellite images. *Nature Cities* (2024). URL <https://www.nature.com/articles/s44284-024-00060-6>.
- [15] Ballinger, O. Open access battle damage detection via pixel-wise *t*-test on Sentinel-1 imagery. *arXiv preprint arXiv:2405.06323* (2024). URL <https://arxiv.org/abs/2405.06323>.
- [16] Yun, S.-H. *et al.* Rapid damage mapping for the 2015 M w 7.8 Gorkha earthquake using synthetic aperture radar data from COSMO-SkyMed and ALOS-2 satellites. *Seismological Research Letters*

**86**, 1549–1556 (2015).

- [17] Tay, C. W. J. *et al.* Rapid flood and damage mapping using synthetic aperture radar in response to typhoon Hagibis, Japan. *Scientific Data* **7** (2020). URL <http://dx.doi.org/10.1038/s41597-020-0443-5>.
- [18] Ge, P., Gokon, H. & Meguro, K. A review on synthetic aperture radar-based building damage assessment in disasters. *Remote Sensing of Environment* **240**, 111693 (2020).
- [19] Copernicus Programme, E. S. A. Sentinel-1. URL <https://sentinels.copernicus.eu/web/sentinel/missions/sentinel-1>.
- [20] Gorelick, N. *et al.* Google Earth Engine: Planetary-scale geospatial analysis for everyone. *Remote Sensing of Environment* **202**, 18–27 (2017). URL <https://doi.org/10.1016/j.rse.2017.06.031>.
- [21] Overture Maps Foundation. Open Map Data. URL <https://overturemaps.org/>.
- [22] Sticher, V., Wegner, J. D. & Pfeifle, B. Toward the remote monitoring of armed conflicts. *PNAS Nexus* **2** (2023). URL <http://dx.doi.org/10.1093/pnasnexus/pgad181>.
- [23] Brown, C. F. *et al.* Dynamic World, near real-time global 10 m land use land cover mapping. *Scientific Data* **9**, 251 (2022).
- [24] Schiavina, M., Melchiorri, M. & Pesaresi, M. GHS-SMOD R2023A – GHS settlement layers, application of the degree of urbanisation methodology (stage I) to GHS-POP R2023A and GHS-BUILT-S R2023A, multitemporal (1975-2030). European Commission Joint Research Centre (2023). URL <http://data.europa.eu/89h/a0df7a6f-49de-46ea-9bde-563437a6e2ba>.
- [25] Miller, E., Kishi, R., Raleigh, C. & Dowd, C. An agenda for addressing bias in conflict data. *Scientific Data* **9**, 593 (2022). URL <https://www.nature.com/articles/s41597-022-01705-8>.
- [26] OpenStreetMap contributors. OpenStreetMap. URL <https://www.openstreetmap.org>.
- [27] Microsoft. Global ML Building Footprints. URL <https://github.com/microsoft/GlobalMLBuildingFootprints>.
- [28] Li, H. Smile - statistical machine intelligence and learning engine. URL <https://haifengl.github.io> (2014).

## Appendix A UNOSAT Dataset

Our reference dataset has been created by combining all existing UNOSAT datasets for Ukraine. We combined them into 18 distinct areas of interest (AOIs). For our purposes, we only use the two strongest labels, *destroyed* and *severely damaged*. For the sake of completeness, we also report the third one here, *moderately damaged*. For Mariupol and Kharkiv, for which multiple analyses were conducted by UNOSAT, we keep only the latest label assigned to a point, assuming that in the case of repeated assessments, the annotations were progressively refined. Table A1 summarizes our AOIs and the number of labeled locations in each of them.

AOI ID	Locations	UNOSAT product ID	# Destroyed	# Severely damaged	# Moderately damaged	Total
UKR1	Mariupol	3371, 3300	365	2184	3102	5651
	Azovstal	3358				
UKR2	Vorzel	3356	647	1116	670	2433
	Hostomel	3359				
	Irpin	3360				
	Bucha	3363				
	Moschun	3417				
UKR3	Rubizhne	3414	700	3182	1041	4923
	Lysychansk	3444				
	Sievierodonetsk	3446				
UKR4	Volnovakha	3415	263	541	66	870
UKR5	Avdiivka	3443	36	505	86	627
UKR6	Chernihiv	3354	266	374	256	896
UKR7	Kharkiv	3357, 3455, 3454	56	168	241	465
UKR8	Borodyanka	3355	43	55	58	156
UKR9	Makariv	3403	18	64	21	103
UKR10	Mykolaiv	3404	33	66	14	113
UKR11	Shchastia	3405	4	12	1	17
UKR12	Sumy	3406	3	6	10	19
UKR13	Trostanets	3407	12	29	6	47
UKR14	Kramatorsk	3408	5	25	8	38
UKR15	Okhtyrka	3413	10	20	9	39
UKR16	Kherson	3436	6	90	9	105
	Antonivka	3435				
UKR17	Kremenchuk	3437	1	7	3	11
UKR18	Melitopol	3442	3	19	13	35
<b>Total</b>			2471	8463	5614	16548

**Table A1** Summary of the 18 distinct areas of interest (AOI) in Ukraine, merging data from 29 UNOSAT products. The table lists counts of destroyed, severely damaged, and moderately damaged labels per area, totaling 16,548 labeled damage instances, or 10,934 after excluding the moderately damaged ones.

## Appendix B Detailed Comparison with the PWTT Baseline

The Pixel-Wise T-Test (PWTT), proposed in [15], is a statistical approach designed to identify changes by comparing the mean values of two Sentinel-1 amplitude time series, adjusted by their standard deviation. We use it as a performance baseline since it utilizes the same data and has similar specifications, in particular, the scalability to large regions and the ease of deployment on GEE.

The PWTT can be calibrated to various conflict settings by optimizing a threshold value to fit existing damage assessments like our UNOSAT labels. For Ukraine in particular, the authors reported an optimal cutoff value of 1.63, based on data from eight different cities. However, their reported results cannot be directly compared to ours as they used different temporal ranges and different training examples for the *undamaged* category: they assume that every building footprint without a damage label from UNOSAT is intact, disregarding the fact that damages could have occurred after the date of the UNOSAT analysis, or could have been overlooked.

For a meaningful comparison, we keep the recommended, optimal cutoff value but rerun PWTT using our time periods and our own, stricter definition of negative labels. We report the corresponding results in Table B2. For readability, we repeat our results in Table B3. It should be noted that Chernihiv and Kharkiv, which represent 61% of our test set, were used by the original authors during the calibration of the PWTT. Nevertheless, our method consistently outperforms the baseline across all metrics.

Label	Precision	Recall	F <sub>1</sub>	F <sub>0.2</sub>	Accuracy	AUC
Damaged	61.9	76.3	68.4	62.4	75.5	75.7
Undamaged	85.6	75.1	80	85.2		

**Table B2** Quantitative performance of the PWTT approach on our test set, with the cutoff value of 1.63 as recommended for Ukraine. All metrics are given as percentages.

Label	Precision	Recall	F <sub>1</sub>	F <sub>0.2</sub>	Accuracy	AUC
Damaged	69.7	78.7	73.9	70.0	80.7	80.3
Undamaged	87.8	81.8	84.7	87.6		

**Table B3** Quantitative performance of our approach on our test set, with confidence threshold 0.5. All metrics are given as percentages.

## Appendix C Choice of optimal threshold

There is an inherent trade-off between precision and recall, and the optimal threshold depends on the specific application. To minimize false alarms in our analysis, we optimized the  $F_{0.2}$ -score for the figures presented in this paper, and found an optimal confidence threshold of 0.64. In practice, users of our tool can dynamically adjust the confidence threshold to suit their specific needs. Fig. C1 illustrates how our metrics vary with different thresholds.

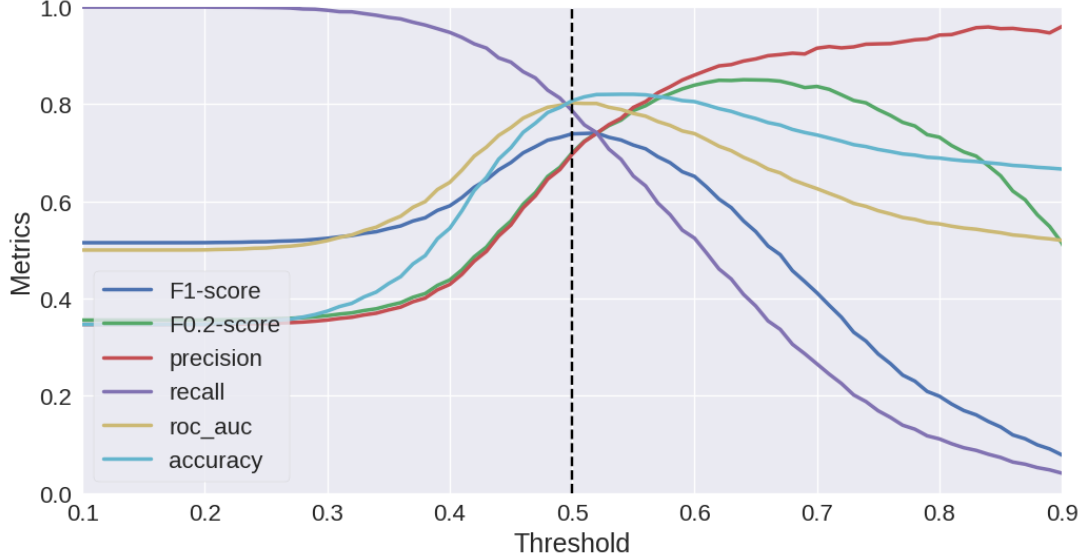


**Fig. C1** Pixel-level performance of our method on our test set, for different confidence thresholds. We find that a confidence threshold of 0.64 optimizes the  $F_{0.2}$ -score.

## Appendix D Temporal Evolution of Damage

The series of maps in Figure Fig. D2 illustrates the progression of building damage over the first two years of the conflict. The maps clearly delineate the primary locations of battles and the frontline, highlighting the areas most affected as the conflict persists.

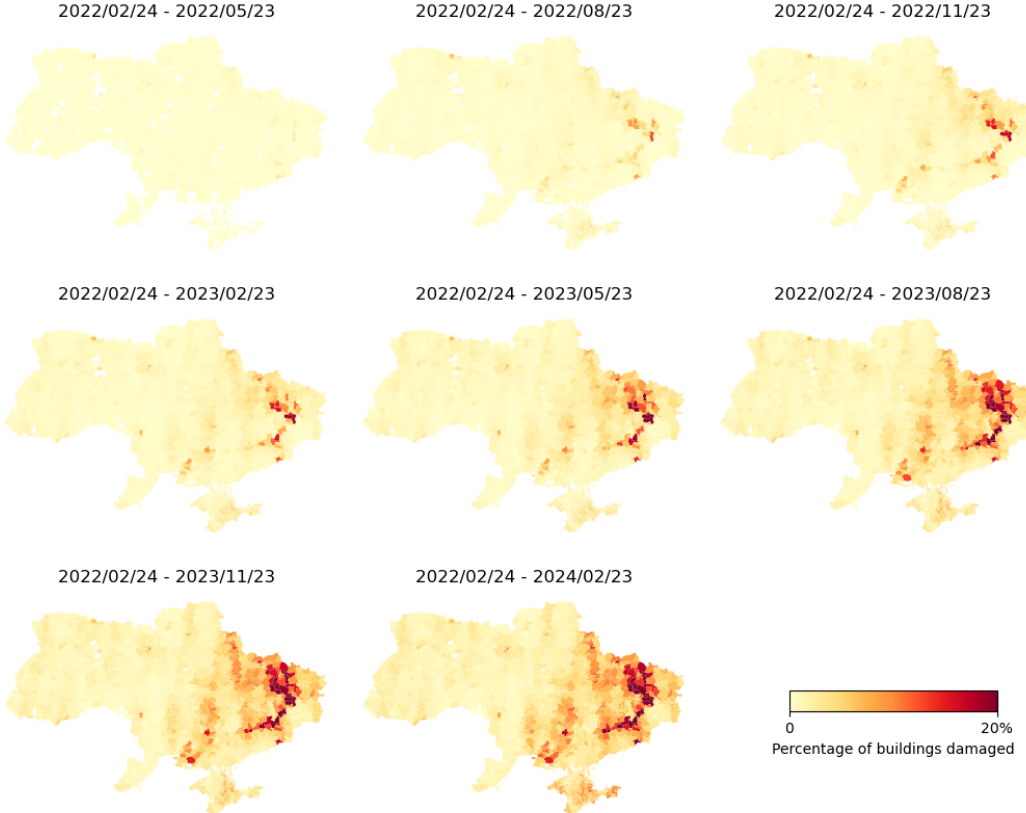


**Fig. D2** Percentage of buildings likely damaged for each period, cumulated since the beginning of the war and aggregated by *hromadas*. The predictions were thresholded at 0.64, and only buildings larger than  $50\text{ m}^2$  were considered.

## Appendix E Limitations of Building Footprints

The building footprints provided by Overture Maps, which for Ukraine were compiled from OpenStreetMap and Microsoft, inevitably come with limitations. For instance, OpenStreetMap data may be obsolete due to the demolition of older structures (Fig. E3.A) or the construction of new ones (Fig. E3.B). While Microsoft footprints serve as a valuable complement to OpenStreetMap data, they were automatically retrieved with a deep neural network from Bing Maps imagery, which may not always offer recent images, and suffers from gaps due to cloudy or outdated acquisitions as for example in Kherson (Fig. E3.C). Moreover, it is not uncommon for large non-building structures, e.g. containers (Fig. E3.D), boats (Fig. E3.E) or even aircraft (Fig. E3.F), to be wrongly identified as buildings.



**Fig. E3** Quality issues of existing building footprints. All images cover  $500 \times 500 \text{ m}^2$  and are displayed alongside the corresponding building footprints sourced from Overture Maps. Only buildings larger than  $50 \text{ m}^2$  are depicted. (A) Outdated buildings in Sevastopol. (B) Absent shopping mall near Chernihiv. (C) Missing footprints in Kherson. (D) Containers in Odessa. (E) Boats in Zaporizhzhia. (F) Antonov International Airport, Hostomel. Satellite images were obtained from ESRI (A and C), Bing (B, E, and F), and Google (D).

## Appendix F World Bank Estimates

The World Bank's third Rapid Damage and Needs Assessment estimated that 547,000 buildings have been completely destroyed in the Ukrainian conflict as of December 31, 2023 [2, p. 76], which aligns with our estimates of over 500,000 buildings damaged over the first two years of conflict.

Furthermore, the report highlights that over 75% of the damage is concentrated in the following oblasts: Donetska (30 %), Kharkivska (27 %), Luhanska (12 %), and Kyivska (8 %). An additional 18 % of the destruction is distributed among Mykolaivska (4 %), Chernihivska (4 %), Khersonska (4 %), Zaporizka (3 %), and Dnipropetrovska (3 %). Fig. F4 shows the differences between those estimates and ours.

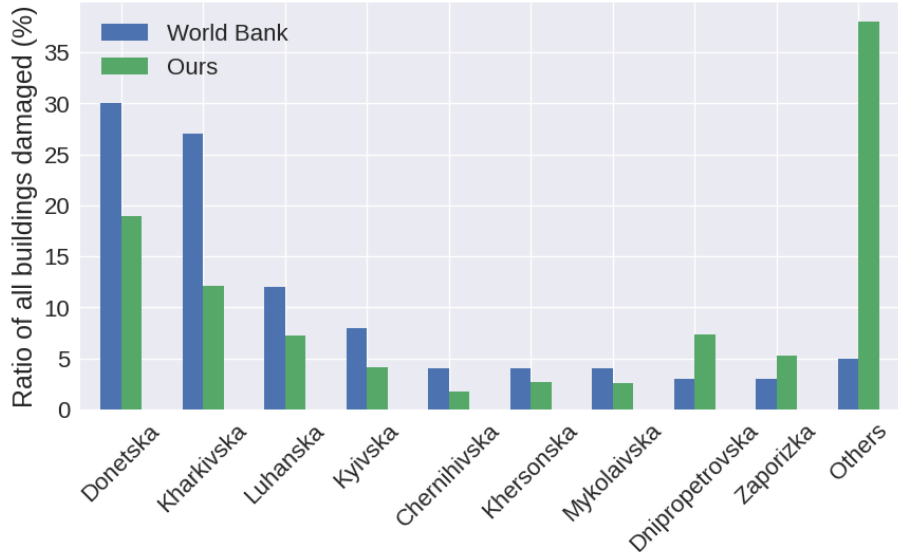


**Fig. F4** Comparison of the World Bank damage distribution by oblasts against our estimates.